Nuclear Instruments and Methods in Physics Research B 269 (2011) 1310–1315

Contents lists available at ScienceDirect

Nuclear Instruments and Methods in Physics Research B

journal homepage: www.elsevier.com/locate/nimb

Solar-wind protons and heavy ions sputtering of lunar surface materials

A.F. Barghouty [a,*], F.W. Meyer [b], P.R. Harris [b], J.H. Adams Jr. [a]

[a] Space Science Office, NASA-Marshall Space Flight Center, Huntsville, AL 35812, USA
[b] Physics Division, Oak Ridge National Laboratory, Oak Ridge, TN 37831, USA

ARTICLE INFO

Article history:
Received 3 November 2010
Received in revised form 8 December 2010
Available online 21 December 2010

Keywords:
Solar wind sputtering
Lunar regolith
KREEP soil
Potential sputtering
Sputtering timescale
Non-equilibrium elemental abundances
Hydrogen deposits on the moon

ABSTRACT

Lunar surface materials are exposed to ~1 keV/amu solar-wind protons and heavy ions on almost continuous basis. As the lunar surface consists of mostly oxides, these materials suffer, in principle, both kinetic and potential sputtering due to the actions of the solar-wind ions. Sputtering is an important mechanism affecting the composition of both the lunar surface and its tenuous exosphere. While the contribution of kinetic sputtering to the changes in the composition of the surface layer of these oxides is well understood and modeled, the role and implications of potential sputtering remain unclear. As new potential-sputtering data from multi-charged ions impacting lunar regolith simulants are becoming available from Oak Ridge National Laboratory's MIRF, we examine the role and possible implications of potential sputtering of Lunar KREEP soil. Using a non-equilibrium model we demonstrate that solar-wind heavy ions' induced sputtering is critical in establishing the timescale of the overall solar-wind sputtering process of the lunar surface. We also show that potential sputtering leads to a more pronounced and significant differentiation between depleted and enriched surface elements. We briefly discuss the impacts of enhanced sputtering on the composition of the regolith and the exosphere, as well as of solar-wind sputtering as a source of hydrogen and water on the moon.

Published by Elsevier B.V.

1. Introduction

The lunar surface is exposed to solar-wind ions on an almost continuous basis. Lacking a global magnetic field as well as a dense atmosphere for protection against these ions, lunar surface material is accessible to solar wind protons and heavy ions with kinetic energies of about 1 keV/amu. At the moon's orbit and during solar minimum conditions, the particle flux in the solar wind is of the order of 10^{12} particles/m^2 s. At the surface, this flux is somewhat reduced due to the shadowing effect of the moon itself but remains largely isotropic. In both charge states and abundances, solar-wind ions reflect the temperature and composition of the lower corona [1]. By number, the proton component is about 93% of the charged-particle flux, while the remaining 7% is distributed among the major solar-wind heavier ions (He through Ar) according to Table 1 [2,3].

At energies around 1 keV/amu, solar-wind protons and heavy ions interact with the lunar surface materials via a number of microscopic interactions [4], but for our purposes here the most important of these is atomic sputtering. Sputtering leads to the removal as well as the introduction of some of the particle species that make up the topmost layers of the lunar surface (regolith). This layer serves as a particle reservoir for the lunar exosphere. Sputtering by solar-wind ions is one of two main mechanisms by which atoms of the top layers are ejected from the surface, the other mechanism being impacts by micro-meteorites [5].

Sputtering may preferentially change the constituents' stoichiometry or chemical composition [6–8]. Depending on their energy and charge state, some of the sputtered species are lost to space while others become part of the lunar exosphere or return to its surface [9–14]. The penetration depth of solar-wind protons and ions at 1 keV/amu (~10 s of nm) is comparable to the thickness of the vapor-deposited layer found on lunar regolith particles [15]. Hence, the properties and composition of this layer (or rim) play critical roles in how the solar-wind ions couple to the lunar surface at the microscopic level.

The timescale of the two erosive processes, solar-wind induced sputtering and micro-meteoritic impacts, is an important characteristic of this dynamic coupling. The timescale for the micro-meteoritic impacts process is estimated to be on the order of thousands of years [16,17]. The timescale for solar-wind sputtering is expected to be much shorter than this since the observed composition of the topmost layer suggests that the solar-wind ions' induced changes reach steady-state faster than the churning effect timescale due to micro-meteoritic impacts [16].

The rim, consisting mostly of oxides, suffers, in principle, both kinetic and potential sputtering. Potential sputtering [18–21] of the lunar surface may be an efficient erosive process. Accurate

* Corresponding author. Tel.: +1 256 961 7508; fax: +1 256 961 7522.
E-mail address: abdulnasser.f.barghouty@nasa.gov (A.F. Barghouty).

0168-583X/$ - see front matter Published by Elsevier B.V.
doi:10.1016/j.nimb.2010.12.033

Table 1
Charge state [2], fraction in the solar-wind flux [3], stored potential energy ($\sum_n E_n$, where E_n is the nth ionization potential), and first ionization potential (FIP) of solar-wind ions.

Ion	Charge state	Fraction	$\sum_n E_n$ (eV)[a]	FIP (eV)
H	1^+	0.93	13.6	13.6
He	2^+	0.04	79.0	24.59
O	$6^+ - 8^+$	7×10^{-4}	1241.5	13.62
C	$4^+ - 6^+$	3×10^{-4}	589.1	11.26
Ne	$7^+ - 9^+$	3×10^{-4}	1431.9	21.56
N	$5^+ - 7^+$	1×10^{-4}	878.0	14.53
Si	$6^+ - 12^+$	3×10^{-5}	1625.8	8.15
Mg	$7^+ - 10^+$	3×10^{-5}	1245.5	7.65
S	$6^+ - 11^+$	1.6×10^{-5}	1246.6	10.36
Fe	$7^+ - 14^+$	8×10^{-6}	1419.8	7.87
Ar	$7^+ - 10^+$	4×10^{-6}	956.6	15.76

[a] This sum is taken to be the arithmetic mean of the sums of the potentials corresponding to the minimum and maximum charge states of the ion as listed in Column 2.

yield estimates of such processes can critically affect estimates of the composition of the lunar regolith and its exosphere. In addition, these yields are expected to be equally important to estimates of the amounts of and sources of hydrogen and water on the surface of the moon. Basic sputtering data and understanding of the relevant sputtering processes is crucial when more precise space measurements, e.g., from the SARA instrument onboard recently launched lunar probe Chandrayaan 1 become available.

As new data from the Oak Ridge National Laboratory's MIRF on potential sputtering of multiply charged ions impacting lunar simulants are becoming available [22], we examine in this contribution the role of potential sputtering in determining the composition of a 'KREEP' surface (materials high in potassium, K, rare Earth elements, 'REE,' and phosphorus, P [9]), which we treat as a proxy of the lunar regolith. We do this using a simple but non-equilibrium model since our objective is to gain a preliminary, qualitative insight into the effects of potential sputtering on the elemental composition of KREEP soil as a function of time. We present this model in the next section along with some preliminary results with and without potential sputtering taken into account. In Section 4 we examine a few possible implications of enhanced sputtering on the composition of the lunar surface, its exosphere, and to sources and estimates of hydrogen deposits on the moon. In Section 5 we offer a summary and some of our preliminary conclusions.

2. Sputtering in a non-equilibrium model

Kinetic sputtering is an inelastic process by which the incoming ion transfers its kinetic energy to a small number of surface atoms via direct, binary collisions [6–8,20,21]. Surface atoms that acquire kinetic energy higher than the surface binding energy (typically only few eVs) will be ejected. Electrons and photons (soft X-rays) can also be ejected but they tend to carry off <5% of the incoming ions' energy [20,21]. Kinetic sputtering is the dominant sputtering mechanism for metals and semiconductors, where any solar-wind induced electronic excitation can be rapidly accommodated [7,8].

In contrast, insulator surfaces, like oxides, have reduced electron mobility, and fast electron removal from the target leads to structural modifications (defects) that cannot be restored, which result in the subsequent desorption of (mostly neutral) particles [7,8]. In this respect, i.e., defect-mediated desorption, potential sputtering is more akin to the processes of electron- and photon-stimulated desorption than to its kinetic sputtering analog [23].

The enhancement observed in the sputter yields for highly charged ions is attributed to the large amount of potential energy they carry; characterized, for example, by the sum of the ionization potentials of the ions [24,25]. Potential sputtering is the dominant sputtering process in insulator materials for highly charged, slow incident ions, i.e., impacting with kinetic energies $\ll$25 keV/amu, and in many cases is significantly more effective in removing target material than kinetic sputtering [7,8].

Accordingly, potential sputtering by the solar-wind heavy ions may significantly alter the total sputter yield of the lunar surface oxides, despite their low abundances relative to protons. This possibility was discussed, at various levels, in Refs. [26–28]: It was dismissed by Wurz et al. [28] based on the assertion that surface metallization would destroy the surface condition required for potential sputtering to occur. Shemansky [27] offered some estimates of potential-sputtering yields to quantify and highlight possible effects on spacecraft skin and environment. Kracher et al. [26] alluded to the effect without offering details.

In order to study the possible dynamic effects of enhanced sputtering yields, we follow here the model proposed in Ref. [16] to study the elemental changes of a KREEP surface exposed to solar-wind protons and heavy ions as a function of time. We assume first that all such changes are due to kinetic sputtering only according to the number-conserving equation:

$$\frac{dC_i}{dt} = \tau^{-1}\left(-C_i \sum_j y_{ij} f_j + C_i^b \sum_{k,j} C_k y_{kj} f_j\right). \quad (1)$$

In the above, C_i is the fractional abundance of element i in KREEP surface soil, C_i^b is the fractional abundance of element i in KREEP bulk, y_{ij} is the yield of element i by solar-wind ion j, and f_j is the fraction of solar-wind ion j in the solar-wind flux (Table 1). We take the KREEP soil to be made up of eleven elements along with their relative abundance ratios as given in Table 2 [9]. The initial condition is defined by $C_i(0) = C_i^b$, where $\sum_1^{11} C_i^b = 1$. Kinetic-sputtering yield data, y_{ij}, are simulated using the SRIM/TRIM simulation package [29], shown in Table 3, which are based on $10^5 - 10^6$ simulated collisional events on an elemental surface made up of the 11 KREEP elements of Table 2. The simulated yields are weighted by the relative abundances. SRIM/TRIM default values for lattice and surface binding energies as well as that for displacements energy were used unchanged.

The constant $\tau = h\rho/J$ has the dimension of time, where h is the penetration depth of solar-wind ions in the KREEP surface ($\sim$100 Å), ρ ($\sim 10^{23}/\text{cm}^3$) is the number density of KREEP, and J the solar-wind flux. Taking a nominal $J \sim 10^8$ ion/cm$^2 - s$, τ is $\sim 10^8$ s. Since the elemental change is modeled on a layer-by-layer basis, as an element i in any particular surface layer is decreased (sputtered), it exposes the bulk element i in a lower layer to further sputtering. This replacement continues until $dC_i/dt = 0$. The characteristic time for element i to reach steady state is $\propto\tau$ divided by its partial yield, $\sum_j y_{ij} f_j$ (normalized to the total sputtering yield, $\sum_{k,j} C_k y_{kj} f_j$).

Table 2
Elemental distribution of KREEP soil [9].

Element	Atomic fraction
O	0.581
Si	0.172
Al	0.065
Ca	0.052
Fe	0.051
Mg	0.048
Ti	0.024
Na	0.004
Cr	0.001
K	0.001
Mn	0.001

Table 3
Kinetic-sputtering yields (in atom/ion) of a KREEP surface by solar-wind protons and heavy ions at 1 keV/amu as simulated by SRIM/TRIM [29].

	O	Si	Al	Ca	Fe	Mg	Ti	Na	Cr	K	Mn
H	.0240	.003865	.001715	.002865	.001345	.002399	.000545	.000261	.000036	.000086	.000043
He	.1486	.0270	.0117	.0175	.008820	.0148	.003790	.001650	.000180	.000620	.000300
O	.9756	.1814	.0760	.1164	.0606	.0974	.0258	.0101	.001430	.003490	.001860
C	.7408	.1394	.0579	.0880	.0463	.0720	.0184	.008040	.001180	.002730	.001080
Ne	1.20	.2243	.0960	.1439	.0742	.1172	.0314	.0129	.001710	.004740	.002300
N	.8503	.1565	.0654	.1004	.0529	.0828	.0228	.008410	.001220	.003200	.001420
Si	1.49	.2750	.1156	.1749	.0920	.1455	.0384	.0153	.002150	.005560	.002780
Mg	1.30	.2384	.1004	.1554	.0804	.1275	.0338	.0143	.001670	.004840	.002380
S	1.67	.3071	.1281	.1992	.1046	.1618	.0432	.0176	.002360	.006210	.002630
Fe	2.37	.4364	.1815	.2779	.1411	.2335	.0590	.0252	.003000	.008870	.004240
Ar	1.80	.2982	.1428	.2134	.1154	.1754	.0488	.0191	.002520	.007830	.003130

Fig. 1 shows results of the compositional change due to solar-wind protons as a function of time (expressed in units of τ) according to Eq. (1). The set of 11 equations based on Eq. (1) are solved numerically. The accuracy of the numerical solution is $\sim 10^{-4}$ and is determined from the constraint that $\sum_1^{11} C_i(t) = 1$ for all t. The proton induced change, $\left[\left(C_i(t) - C_i^b\right)/C_i^b\right] \times 100$, is seen to approach steady-state for times $\approx 300\tau$ whereat oxygen is reduced by 17% while Fe and Al are enhanced by about 30% and Si and Ti by 50%. The abundance-weighted average change for all 11 elements is about 27%. Fig. 2 shows the same when the solar-wind heavy ions are included but only their kinetic sputtering is taken into account. The overall enhancement in the sputtering rate, as calculated by the total sputtering yield ($\sum_{k,j} C_k y_{kj} f_j$), is about 26% higher than that induced by protons only. Time to reach steady-state is $\approx 200\tau$ (compared to $\approx 300\tau$ for protons). The overall steady-state elemental distribution as well as the abundance-weighted average change are, however, largely the same as those induced by proton sputtering.

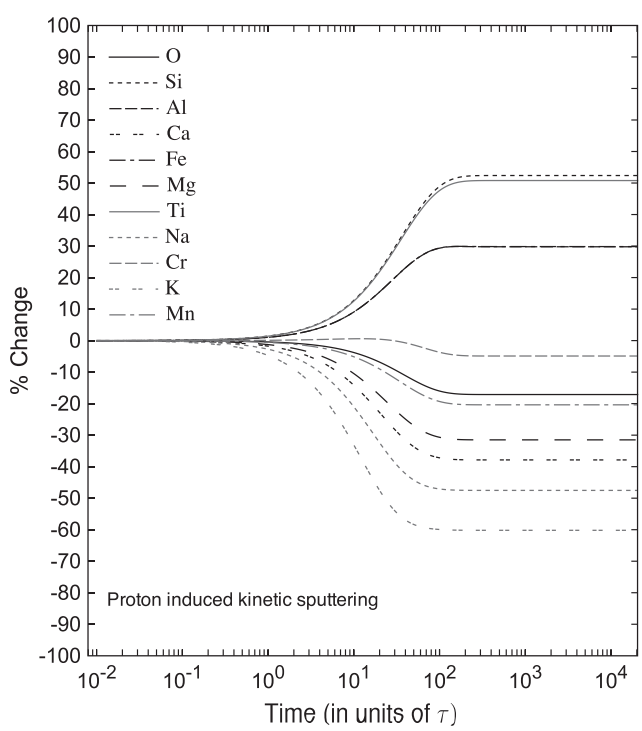

Fig. 1. Calculated changes, $\left[\left(C_i(t) - C_i^b\right)/C_i^b\right] \times 100$, where $C_i(t)$ is the fractional abundance of element i and C_i^b is its corresponding bulk fraction, in the elemental composition of a KREEP surface as a function of time due to kinetic sputtering of the solar-wind protons.

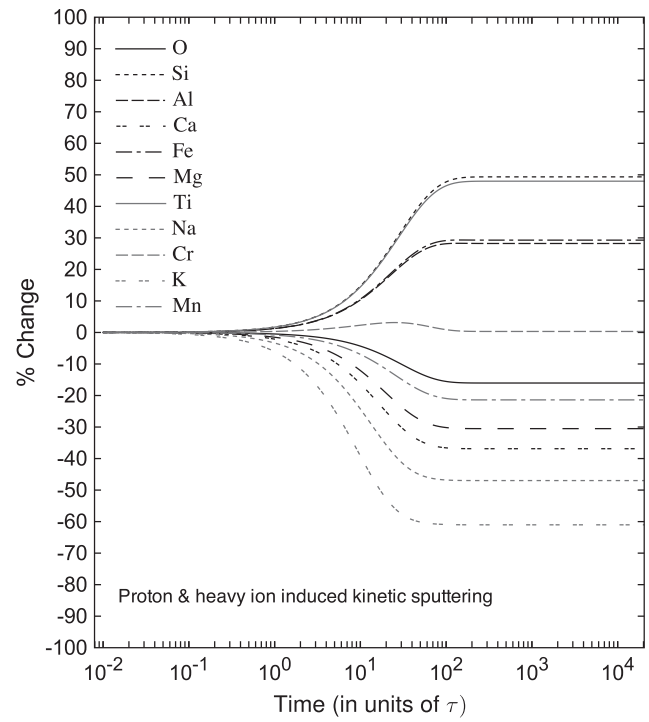

Fig. 2. Calculated changes in the elemental composition of a KREEP surface as a function of time due to the combined kinetic sputtering of the solar-wind protons and heavy ions.

The sputtering rate can increase with a decreasing τ or an increasing total yield. The former requirement, on the one hand, requires a much larger solar-wind flux. The solar-wind flux can be large during solar maximum conditions. But these are transient [30] and of short durations, ~hours to days, relative to a timescale on the order of thousands of years. The total sputter yield, on the other hand, can be enhanced by potential sputtering. We examine next this enhancement and its dynamic effects.

3. Enhanced sputtering in a non-equilibrium model

While the exact enhancement due to potential sputtering is difficult to estimate, for our purposes here, we follow [18] in assuming that the yield due to potential sputtering scales with the total potential energy level of the impacting ion as

$$y_{ij}^{\text{potential}} = \alpha_i \left(\mathcal{E}_j\right)^{\beta_i}, \tag{2}$$

where $\mathcal{E}_j = \sum_n E_n - E_1$ for solar-wind ion j, E_n being its nth ionization potential (see Table 1). The first ionization potential is subtracted so

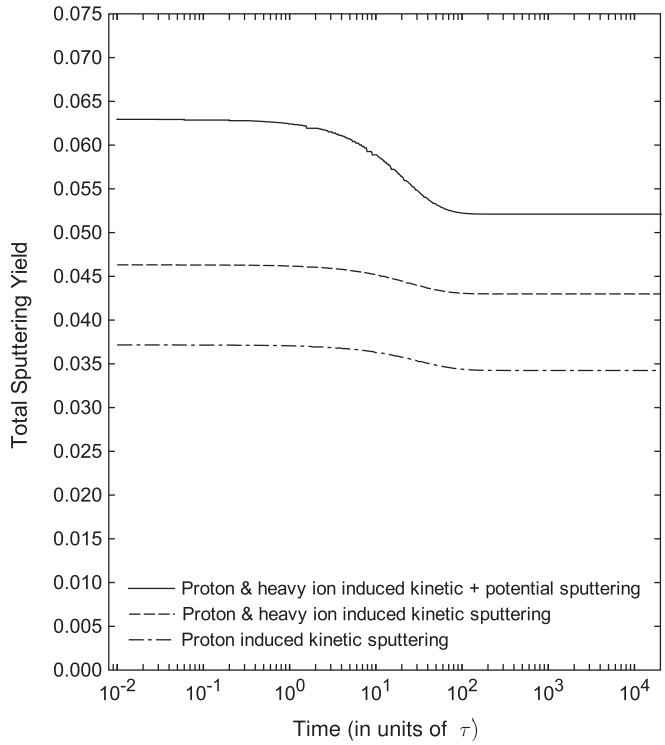

Fig. 3. Calculated total sputtering yield, $\sum_{k,j} C_k y_{kj} f_j$, as a function of time showing the two effects of enhanced sputtering due to the actions of solar-wind heavy ions vs. protons, on the one hand, and kinetic vs. potential sputtering, on the other.

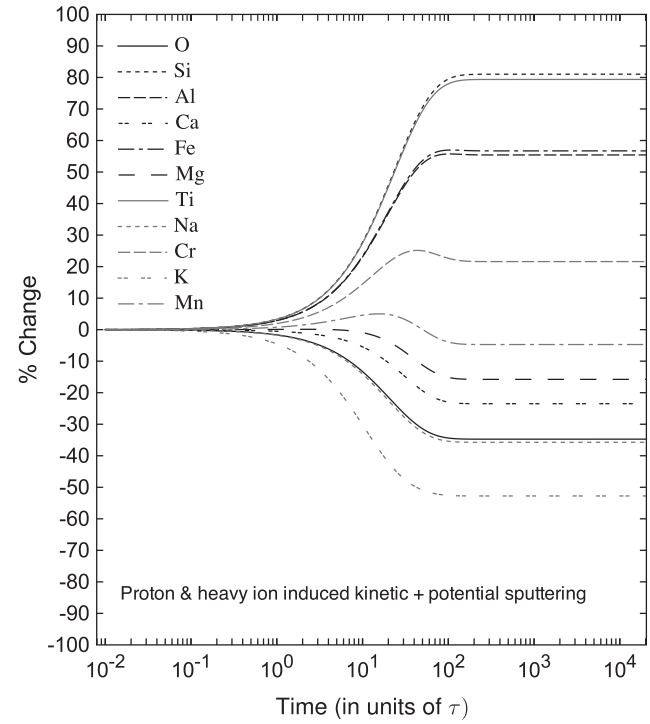

Fig. 4. Calculated changes in the elemental composition of a KREEP surface as a function of time due to the combined kinetic as well as potential sputtering of the solar-wind protons and heavy ions (see text).

that singly-charged ions (including protons) have no potential sputtering contribution. Based on the new Oak Ridge data for Ar-induced oxygen sputtering [22] and the SRIM/TRIM simulations, we find $\alpha_o \approx 3.12$ and $\beta_o \approx .57$ (when $\mathcal{E}_j$ is expressed in keV/amu). For all other KREEP elements we take their $\alpha_i = 0$. We only assume then that, for oxygen, α_o and β_o carry over to other impacting solar-wind ions. The two sputtering yields, kinetic (based on the SRIM/TRIM simulations) and potential (for oxygen as estimated above), are assumed to simply add to the total sputtering yield for each element i due to the actions of ion j as,

$$y_{ij}^{\text{total}} = y_{ij}^{\text{kinetic}} + y_{ij}^{\text{potential}}. \tag{3}$$

We show in Fig. 3 the qualitative effect of enhanced sputtering where the total sputtering yield, $\sum_{k,j} C_k y_{kj} f_j$, is shown as a function of time. Here, again, Eq. (1) is solved for protons and heavy ions and with the total sputtering yields, y_{ij}, estimated as described above. Integrated over time, the overall enhancement due to the actions of heavy ions (but without potential sputtering) is about 26%. When both kinetic and potential sputtering are taken into account, however, the enhancements are about 52% over proton-induced sputtering and about 21% over kinetic sputtering induced by both protons and heavy ions. While the inclusion of heavy ions (without potential sputtering) has significantly shortened the characteristic timescale (by 33%), the added enhancement associated with potential sputtering shortened this scale by only another 5% or less. This is easily appreciated as being due to the fact that enhanced depletion in one or more elements (i.e., oxygen here) will have to be accompanied by enhanced enrichment in others (e.g., Fe and Si); it is the net effect that determines the timescale, rather than the average effect.

Fig. 4 shows results of our preliminary calculations for the elemental changes of KREEP as functions of time when both kinetic and potential sputtering are taken into account. Compared to those changes depicted in Fig. 2, where only kinetic sputtering is taken into account, the reduction in O is now at 35% compared to 17% while it is 23% vs. 37% for Ca, 16% vs. 31% for Mg, and 36% vs. 47% for Na. This is accompanied by marked enhancements for Si (81 vs. 49%), Fe (57 vs. 30%), Ti (79 vs. 48%), and Al (55 vs. 28%). The abundance-weighted average change for all 11 elements is about 45% (compared to 26%). The distribution of depleted vs. enriched elements depicted in Figs. 2 and 4 are qualitatively consistent with observations [31,32]. The net effect of potential sputtering appears to be a more pronounced and significant differentiation between depleted and enriched elements. We briefly examine next some possible implications of this enhanced sputtering.

4. Possible implications of enhanced sputtering

4.1. To the composition of the lunar regolith

In a detailed study of how the erosive and selective nature of solar-wind sputtering affects the composition of the lunar regolith, Starukhina [16] arrived at and used an erosion rate of about 0.2 Å/year. It was assumed that the solar-wind heavy ions contribute collectively about 30% of the proton-induced yield. This 30% increase was argued for on the basis that solar-wind heavy ions add to the total yield via the ions increased mass, i.e., kinetic sputtering only. In this estimate of the erosion rate potential sputtering was not taken into account. (Note that according to Fig. 3, in our model the corresponding increase is about 26% without potential sputtering and 52% with.)

The same study calculated the contribution of solar-wind sputtering to the elemental abundance of lunar regolith, focusing on Fe and H. The study found that selective sputtering increases the concentration of iron in the rims while decreasing other elements like calcium. It was found that sputtering, together with impact evaporation, lead to large and small scale mixing of rim material and, thus, to an averaging of the rim elemental composition. If potential

sputtering were to contribute to the total yield in the fashion suggested by our simple model above, i.e., 52% increase over the proton induced yield, the erosion rate estimated by Starukhina [16] would increase proportionally because of the linear relationship between yield and erosion rate, leading to an even more efficient mixing. In addition, and as importantly, the sputtering timescale, as demonstrated earlier, would decrease. As a result, the simulated surface composition should be more rapidly changed than would be expected on the basis of kinetic sputtering alone.

4.2. To the composition of the lunar exosphere

As alluded to earlier, along with the action of micro meteorites' impacts, solar-wind ions collisions with lunar surface materials are believed to be the two main mechanisms by which the composition of the upper most layers of the lunar regolith are altered [9]. Solar-wind induced sputtering ejects surface and near-surface species into the exosphere with a rather broad energy distribution. In addition to changes to the surface materials due to prolonged and preferential erosion, solar-wind induced sputtering is also expected to contribute to the elemental composition of the exosphere [5]. The study in [28] examined in detail the contribution of solar-wind proton-induced kinetic sputtering to elemental densities found in the exosphere, both at the surface and as a function of height above the surface.

This study found that solar-wind induced sputtering contributes only about 10 atoms/cm^3 to an observed exospheric surface density of about 10^6 atoms/cm^3 [14]. The calculated elemental abundances, according to the same study, was generally 'consistent' with the measured ones in the sense that the calculated ones were well below the observed upper limits. The study concluded that the lunar exosphere is dominated by elements released thermally and by the process of photon-stimulated desorption, rather than by solar-wind induced sputtering or micro-meteoritic impacts.

The above mentioned study dismissed any contribution of potential sputtering to the total yield on the basis that potential sputtering is dose sensitive. They argued that the solar-wind dose is such that in a matter of only 2 months, solar-wind heavy ions would have preferentially removed enough oxygen from the surface monolayer, i.e., making it more conductive, so that the effects of potential sputtering are reduced to that of kinetic sputtering. This dose-dependent timescale being much smaller than other timescales, led [28] to conclude that the contribution of solar-wind heavy ions to the total sputter yield, i.e., potential sputtering, could be neglected.

We believe that this 'dosing' effect, while inferred in the laboratory for some surfaces [24], may not be relevant to solar-wind lunar-surface interactions. Lunar regolith surface metallization would have been significantly reduced due to sputtering by protons, the dominant component of the solar wind, which is much less mass selective; the overall decrease of the surface oxygen concentration may thus be too small to cause surface metallization. Additionally, in the new measurements [22] for lunar regolith simulant no such effect was observed. Contribution of potential sputtering to the composition of the lunar regolith and its exosphere cannot, we believe, be dismissed on the basis of the dosing effect seen in laboratory studies alone. Thus potential-sputtering contribution needs to be looked at more carefully, e.g., with time dependent calculations, and especially in light of the preliminary data from ORNL [22].

4.3. To estimates and sources of hydrogen deposits on the moon

It is estimated [5,12,13] that most of the solar-wind protons impacting the lunar surface are implanted, and, thus, are able to act as a source for hydrogen on the moon [5,10,11,16,17]. Bombardment by solar-wind ions releases this implanted hydrogen component which can subsequently migrate to the poles, or react and form hydrogen molecules in the surface. Models for the estimates of the hydrogen and ice deposits depend sensitively on the solar-wind sputter yields. To illustrate, using a sputter yield of only 10^{-4} H atom per incoming solar-wind proton, Refs. [10,11] deduced a total hydrogen delivery to the lunar poles of 1.2×10^{-2} H atom/proton. Of this, they estimate that about 0.4% actually gets trapped as frozen water in the permanently shielded cold traps at the lunar poles. Given the solar-wind flux, this translates into about 4 tons of water per year delivered by the solar-wind protons to the lunar poles. In Ref. [17], on the other hand, using kinetic sputtering yields along with an estimate for the backscatter fraction, it is estimated that the same hydrogen delivery at the lunar poles is only $\sim 10^{-4}$ H atom/proton.

When considering the possibility of additional sputtering mechanisms being active, the uncertainty of such estimates may well be even larger. In the former estimates, a mere downshift of 50% in the hydrogen deposition rate (due to more efficient sputtering of H atoms with broad energy distribution by the solar-wind ions) reduces the estimated tonnage of water at the poles by a factor of 4 (assuming independent escape and migration processes as done in their study). Remarkably, a factor of 10 increase, as has been reported for some surfaces [33,34], in the sputtering efficiency of implanted hydrogen reduces the amount of trapped H to that of the bulk material (i.e., <100 ppm [9]).

Using steady-state estimates, the simulations in [16] found that the amount of implanted H that is either solar-wind sputtered or backscattered is too little to account for the hydrogen estimates at the lunar poles. As an alternative source for this hydrogen, [16] suggests that the earth's magnetotail is a more likely source because of its much larger hydrogen content.

An enhanced sputter yield due to potential sputtering would lead to an enhanced H delivery at the lunar poles only if the energy distribution is assumed to be similar to that for kinetic sputtering (so that not many sputtered atoms are lost to outer space), and if the enhancement observed in proton sputtering is accompanied by an enhancement of the total H atom sputtering yield. If the energies of potentially-sputtered H atoms are substantially greater, less will be captured by the lunar gravity resulting in a decrease of H delivery at the lunar poles. While an increase in the backscatter fraction would be able to counteract such a drop, it is not clear whether this increase would be sufficient [16]. Hence, the inclusion of potential sputtering is likely to result in a smaller contribution to hydrogen deposits that can be attributed to solar-wind sputtering, which would make the earth's magnetotail a more likely source of hydrogen and water on the moon.

5. Summary and conclusions

Sputtering is an important, dynamic mechanism that affects the composition of both the lunar surface and its tenuous exosphere. While the contribution of solar-wind protons and ions' kinetic sputtering to the changes in the composition of the surface layer of the oxides of the lunar surface is well understood and modeled, role and implications of potential sputtering remain unclear, mostly due to lack of relevant measurements.

New data from Oak Ridge National Laboratory's MIRF on potential sputtering of multi-charged ions impacting lunar simulants are becoming available [22]. In anticipation of such data, we have examined in this contribution the role and some possible implications of potential sputtering of Lunar KREEP material by protons as well as by the major heavy-ion component of the solar wind. Using a non-equilibrium model we have demonstrated that solar-wind heavy ions, without their potential sputtering contribution, contribute about 26% of the proton induced yield. With potential sputtering, they contribute about 52% of the proton yield. This

enhanced sputtering leads to a more pronounced and significant differentiation between depleted and enriched surface elements. We have also shown that the timescale of the overall sputtering process can be significantly shortened when contribution of the heavy-ion component of the solar wind is taken into account.

While more detailed calculations and modeling of the impacts of enhanced sputtering will be based on the new ORNL data, our preliminary calculations suggest that enhanced sputtering can lead to more efficient and rapid mixing of the composition of the lunar regolith. The contribution of solar-wind sputtering to the composition of the lunar exosphere needs to revisited in light of both the enhanced sputtering as well as reduced timescale. Finally, more efficient erosion of hydrogen from the lunar surface associated with enhanced sputtering may suggest that the earth's magnetotail could be a more likely source of hydrogen and water deposits on the moon than the solar-wind proton and ions' induced sputtering.

Acknowledgements

AFB wishes to extend his sincere thanks and appreciation to the organizers of IISC-18 (Drs. Fred Meyer and Carlos Reinhold in particular) for their gracious invitation as well as for their continued support of this effort at both Oak Ridge and Marshall.

References

[1] H. Zirin, Astrophysics of the Sun, Cambridge Univ. Press, Cambridge, England, 1988.
[2] R. von Steiger, N.A. Schwadron, L.A. Fisk, J. Geiss, G. Gloecker, S. Hefti, B. Wilken, R.F. Wimmer-Schweingruber, T.H. Zurbuchen, J. Geophys. Res. 105 (2000) 27. 217.
[3] S.J. Bame, J.R. Asbridge, W.C. Feldman, M.D. Montgomery, P.D. Kearney, Solar Phys. 43 (1975) 463.
[4] C. Lemell, M. Alducin, J. Burgdörfer, J.I. Juaristi, K. Schiessl, B. Solleder, K. Tokesi, Rad. Phys. Chem. 76 (2007) 412.
[5] R.R. Hodges Jr., The Moon 14 (1975) 139.
[6] P. Sigmund, in: R. Behrisch (Ed.), Sputtering by Ion Bombardment: Theoretical Concepts, vol. I, Springer, Berlin, 1981.
[7] T. Schenkel, A.V. Hamza, A.V. Barnes, D.H. Schneider, Prog. Surface Sci. 61 (1999) 23.
[8] F. Aumayr, H. Winter, Nucl. Instrum. Methods B 233 (2005) 111.
[9] G.H. Heiken, D.T. Vaniman, B.M. French, Lunar Source Book: A User's Guide to the Moon, Cambridge Univ. Press, Cambridge, England, 1991. Chap. 7.
[10] D.H. Crider, R.R. Vondrak, Adv. Space Res. 30 (2002) 1869.
[11] R.R. Vondrak, D.H. Crider, Am. Sci. 91 (2003) 322.
[12] J.R. Arnold, J. Geophys. Res. 84 (1979) 5659.
[13] B.J. Butler, J. Geophys. Res. 102 (1997) 283.
[14] S.A. Stern, Rev. Geophys. 37 (1999) 453.
[15] Y. Liu, J. Park, E. Hill, K.D. Kihm, L.A. Taylor, in: Space 2006, ASCE Proc., Houston, 2006.
[16] L.V. Starukhina, Solar Syst. Res. 37 (2003) 36.
[17] L.V. Starukhina, Y.G. Shkuratov, Icarus 147 (2000) 585.
[18] M. Tona, S. Takahashi, K. Nagata, N. Yoshiyasu, C. Yamada, N. Nakamura, O. Shumsuki, Appl. Phys. Lett. 87 (2005) 224102-1–224102-3.
[19] F. Aumayr, H. Winter, Phil. Trans. R. Soc. Lond. A 362 (2004) 77.
[20] R.A. Baragiola, Phil. Trans. R. Soc. Lond. A 362 (2004) 29.
[21] M.W. Thomson, Vacuum 66 (2002) 99.
[22] F.W. Meyer, R.P. Harris, C.N. Taylor, H.M. Meyer III, A.F. Barghouty, J.H. Adams Jr., these proceedings.
[23] J. Burgdörfer, Y. Yamazaki, Phys. Rev. A 54 (1996) 4140.
[24] G. Hayderer, M. Schmidt, P. Varga, H. Winter, F. Aumayr, L. Wirtz, C. Lemell, J. Burgdörfer, L. Hagg, C.O. Reinhold, Phys. Rev. Lett. 83 (1999) 3948.
[25] G. Hayderer, S. Cernusca, V. Hoffmann, D. Neimann, N. Stolterfoht, M. Schmid, P. Varga, H.P. Winter, F. Aumayr, Nucl. Instrm. Methods B 182 (2001) 143.
[26] A. Kracher, F. Aumayr, D.W.G. Sears, M. Kareev, Meteoritics and Planetary Science, vol. 38, Supplement, Abstract No. 5204, 2003.
[27] D.E. Shemansky, in: A.D. Ketsdever, E.P. Muntz (Eds.), Rarefied Gas Dynamics, vol. CP663, AIP, Wash., DC, 2003.
[28] P. Wurz, U. Rohner, J.A. Whitby, C. Kolb, H. Lammer, P. Dobniker, J.A. Martin-Fernandez, Icarus 191 (2007) 486.
[29] J.F. Ziegler, J.P. Biersack, U. Littmark, The Stopping and Range of Ions in Solids, Pergamon, New York, 1996. Available from: <http://www.srim.org>.
[30] D.V. Reames, Space Sci. Rev. 90 (1999) 413.
[31] T. Gold, E. Bilson, R.L. Baron, in: Proc. 6th Lunar Sci. Conf., 1975, p. 3285.
[32] Yu.P. Dikov, O.A. Bogatikalov, V.L. Baruskov, F.P. Florensky, A.V. Ivanov, V.V. Nemeshkalenko, V.G. Alyoshin, M.G. Chudinov, in: Proc. 9th Lunar Sci. Conf., 1978, p. 2111.
[33] M. Kakutani, Y. Azuma, K. Komaki, K. Kuroki, Nucl. Instrum. Methods B 96 (1995) 541.
[34] Y. Yamazaki, K. Kuroki, Curr. Opin. Solid State Mater. Sci. 6 (2002) 169.